applied sciences

MDPI

Article

Intelligent Classification of Tunnel Surrounding Rock Based on Tunnel Face Image Recognition

JiaJun Fu [1], Fuchun Sun [1], Weisheng Li [2,*] and Chenda Xie [2]

[1] Department of Computer Science and Technology, Tsinghua University, Beijing 100084, China
[2] School of Civil Engineering, Central South University, Changsha 410075, China
* Correspondence: 15115917230@163.com; Tel.:+86-15115917230

Abstract

Purpose—Accurate classification of tunnel surrounding rock is essential for safe excavation, timely support adjustment, and risk control during construction. This study proposes an intelligent classification method that links tunnel face image recognition with a modified BQ rock-mass quality framework. Design/methodology/approach—A YOLOv8 model was trained to detect and localize joints and fractures on tunnel face photographs. The detected fracture regions were processed through grayscale conversion, denoising, histogram equalization, adaptive thresholding, and morphological operations. Pixel statistics were used to calculate the fracture-area ratio and derive a crack ratio for evaluating tunnel face integrity. The image-derived integrity coefficient, rebound-test-based saturated uniaxial compressive strength, and correction coefficients were integrated to calculate the corrected BQ value. Findings—The method was validated using data from the Laimipo Tunnel in Yueyang, China. The YOLOv8 model identified tunnel face joints and fractures effectively, with a mean average precision (mAP@0.5) value of 0.898 for the fracture class. Field validation on ten tunnel faces showed that the predicted surrounding rock grades were consistent with the measured grades in nine cases, giving an accuracy of 90%. Originality/value—The study links image-based fracture recognition with the modified BQ method and provides a rapid, quantitative workflow for construction-stage surrounding rock classification and timely support adjustment.

Keywords: surrounding rock classification; image recognition; modified BQ method; tunnel support

1. Introduction

The stability of surrounding rock is critical during tunnel excavation, and tunnel support design depends on accurate classification of tunnel surrounding rock quality [1,2]. Since the concept of surrounding rock classification was proposed in 1774, many scholars have developed rock mass classification methods from the perspectives of influencing factors and classification criteria. Representative systems include the rock structure rating (RSR) [3], the rock mass rating (RMR) [4], the Q system [5], and the rock quality designation (RQD) [6]. In China, commonly used classification methods include the national BQ method [7] and the HC method used in hydropower engineering [8]. For highway and railway tunnels, the surrounding rock quality of tunnel engineering is generally evaluated according to the Standard for Engineering Classification of Rock Mass (GB/T 50218-2014) [7], namely the BQ method. However, although conventional classification

Check for updates

Received: 16 September 2026
Revised: 13 October 2026
Accepted: 19 October 2026
Published: 22 October 2026

Copyright: © 2026 by the authors. Licensee MDPI, Basel, Switzerland. This article is an open access article distributed under the terms and conditions of the Creative Commons Attribution (CC BY) license.

indices have broad applicability, some indices are difficult to obtain under special engineering geological conditions such as karst, extra-large spans, and high ground temperature. As a result, the evaluation results of these classification methods may be poorly applicable and may deviate substantially from field conditions.

Therefore, many researchers have improved and optimized rock mass quality classification methods for different tunnel characteristics. Tu et al. [9] argued that conventional rock mass quality classification neglects the effects of uncertainty and complexity on tunnel surrounding rock classification, and introduced dynamic weighting and extension methods to improve rock mass quality assessment. Jiang et al. [10] proposed a rock mass quality evaluation method based on fuzzy reasoning and support vector machines, which reduces interpretive bias in subjective parameters. He et al. [11] proposed a rapid rock mass quality evaluation method based on multi-source heterogeneous data screening and a Gaussian process classification model to overcome the low accuracy of single-factor evaluation and the lithology dependence of multi-factor evaluation. Aydan et al. [12] proposed a new rock mass quality rating system, termed the rock mass quality rating method (RMQR), for estimating rock mass properties and achieving rock mass quality classification.

Some researchers have attempted to revise tunnel surrounding rock classification by combining advanced geological prediction, image photography, and actual field exposure of surrounding rock [13,14]. Sun et al. [15] developed technical operating standards for tunnel face surveying based on digital photogrammetry, constructed 62 three-dimensional tunnel face models, and systematically analyzed the quantitative relationships among surrounding rock grade, joint parameters, and contour characteristics using fractal dimensions. Hou et al. [16] used a three-dimensional digital photography system to collect geometric information on rock mass structural planes, quantified the geological strength index by combining volumetric joint count and joint roughness coefficient, and completed analysis of surrounding rock mechanical parameters based on the Hoek-Brown criterion to support stability evaluation. Ma et al. [17] constructed an HRNet-BO intelligent surrounding rock classification model based on TBM operational parameters by using Bayesian optimization to simultaneously optimize the network structure and hyperparameters; compared with conventional models, the model showed better learning and generalization ability. Zhang et al. [18] fused tunnel face images with ground-penetrating radar advanced geological prediction data and, together with field geological survey results from surrounding rock exposure, proposed a deep learning-based dynamic surrounding rock classification method for the construction stage, thereby compensating for the strong subjectivity and insufficient intelligence of conventional classification methods.

Overall, with the continuous development of intelligent tunnel construction, digital acquisition and intelligent analysis technologies have been widely introduced into key tasks such as rock mass parameter acquisition, mechanical-property analysis, and surrounding rock quality classification. These technologies have significantly improved evaluation efficiency and discrimination accuracy and have become important technical support for safe and efficient tunnel construction. In surrounding rock classification, the introduction of artificial intelligence has rapidly become a research focus and development trend, producing many innovations based on deep learning, ensemble learning, and optimization algorithms. Chen et al. [19] proposed an advanced integrated pixel-level method named DeepLabv3+ based on a deep convolutional neural network, which can detect and quantify weak interlayers in tunnel faces and achieves higher accuracy than conventional methods. Zhang et al. [20] used residual learning in a deep convolutional neural network (DCNN) combined with multi-scale dilated-convolution attention blocks to rapidly identify the lithology of tunnel face rock during construction. Liu et al. [21] developed a rock drilling test system that enables real-time and high-precision automatic

acquisition of multiple drilling parameters, and established an intelligent surrounding rock grade recognition model using a random forest algorithm, with an average recognition accuracy greater than 0.9, providing technical support for intelligent drill-and-blast tunnel construction. Niu et al. [22] addressed the recognition of hard structural planes in deep tunnels by proposing an adaptive illumination correction method and a YOLOv8 recognition algorithm integrated with joint completion, which effectively improved structural-plane recognition accuracy and provided a technical basis for intelligent disaster assessment in deep tunnels. Xu et al. [23] proposed an intelligent classification method combining a cross-attention Transformer and XGBoost to address limitations in existing TBM surrounding rock classification methods; by fusing multi-stage tunnelling data, the method balances classification accuracy and interpretability and can support optimization of intelligent TBM tunnelling parameters.

Conventional BQ-based classification is difficult to implement continuously at the tunnel face because rock strength and rock mass integrity are not always available during excavation. Existing image-based methods can identify fractures or structural planes, but their outputs are seldom directly linked to engineering classification indices. This study develops a construction-stage workflow that uses tunnel face images to quantify fracture development and estimate the integrity coefficient, while rebound testing indirectly obtains saturated uniaxial compressive strength. These parameters and correction coefficients are incorporated into the corrected BQ framework for rapid surrounding rock classification.

2. BQ Classification Method

According to the Standard for Engineering Classification of Rock Mass (GB/T 50218-2014) (MHURDPRC, 2014) [7], the basic quality index of rock mass, BQ, is calculated as follows:

$$\mathrm{BQ} = 100 + 3R_c + 250K_v \quad (1)$$

where BQ is the basic quality index of rock mass; R_c is the uniaxial compressive strength of the rock (MPa); and K_v is the rock mass integrity coefficient.

When Equation (1) is used, two conditions should be noted. If $R_c > 90\ K_v + 30$, $R_c = 90\ K_v + 30$ and K_v should be substituted into Equation (1). If $K_v > 0.04\ R_c + 0.4$, $K_v = 0.04\ R_c + 0.4$ and R_c should be substituted into Equation (1). The BQ-based classification of surrounding rock may refer to the Specification for Design of Highway Tunnels (JTG 3370.1-2018) [24], as shown in Table 1.

Table 1. Surrounding rock classification based on the BQ method.

Quality Grade	Qualitative Characteristics of Basic Rock Mass Quality	BQ Value
I	Hard rock with intact rock mass	>550
II	Hard rock with relatively intact rock mass; relatively hard rock with intact rock mass	550–451
III	Hard rock with relatively fractured rock mass; relatively hard rock with relatively intact rock mass; relatively soft rock with intact rock mass	450–351
IV	Hard rock with fractured rock mass; relatively hard rock with relatively fractured to fractured rock mass; relatively soft rock with relatively intact to relatively fractured rock mass; soft rock with intact to relatively intact rock mass	350–251
V	Relatively soft rock with fractured rock mass; soft rock with relatively fractured to fractured rock mass; all extremely soft rock and extremely fractured rock	≤250

When groundwater, in-situ stress, or dominant structural planes strongly affect the rock mass, classification based only on the BQ value may lead to considerable errors. In such cases, the BQ value should be corrected, and the corrected value [BQ] should be used with Table 1 to determine the surrounding rock grade. The corrected BQ value is calculated as follows:

$$[BQ] = BQ - 100(K_1 + K_2 + K_3) \quad (2)$$

where [BQ] is the corrected basic quality index of rock mass; K_1 is the groundwater correction coefficient; K_2 is the correction coefficient for the occurrence of the dominant structural plane; and K_3 is the correction coefficient for the initial stress state.

According to the specification (MTPRC, 2018) [24], the groundwater correction coefficient K_1 in Equation (2) may be selected from Table 2. If multiple weak structural planes are present, each weak structural plane should be measured, and the corresponding K_2 value should be determined using Table 3. The structural plane with the largest influence coefficient should be selected as the weak structural plane that has the greatest influence on stability. The correction coefficient K_3 for the initial stress state is determined according to Table 4.

Table 2. Correction coefficient K_1 for groundwater influence.

Groundwater Condition	BQ Value				
	>550	550–451	450–351	350–251	≤250
Damp or dripping water $p \leq 0.1$ or $Q \leq 25$	0	0	0–0.1	0.2–0.3	0.4–0.6
Rain-like or linear-flow water $0.1 \leq p \leq 0.5$ or $25 \leq Q \leq 125$	0–0.1	0.1–0.2	0.2–0.3	0.4–0.6	0.7–0.9
Gushing water $p > 0.5$ or $Q > 125$	0.1–0.2	0.2–0.3	0.4–0.6	0.7–0.9	1.0

Note: p is the fissure-water pressure of the surrounding rock in underground engineering (MPa); Q is the water inflow per 10 m tunnel length (L/min per 10 m).

Table 3. Correction coefficient K_2 for the occurrence of weak structural planes.

Relationship Between the Attitude of the Structural Plane and the Tunnel Axis	The Intersection Angle Between Structural Plane Strike and Tunnel Axis < 30°, Dip Angle of Structural Plane 30–75°	The Intersection Angle Between Structural Plane Strike and Tunnel Axis > 60°, Dip Angle of Structural Plane > 75°	Other
K2	0.4–0.6	0–0.2	0.2–0.4

Table 4. Correction coefficient K_3 for the initial stress state.

Initial Stress State		BQ Value				
		>550	550–451	450–351	350–251	≤250
Extremely high stress	Rc/σmax < 4	1.0	1.0	1.0–1.5	1.0–1.5	1.0
High stress	Rc/σmax = 4–7	0.5	0.5	0.5	0.5–1.0	0.5–1.0

The modified BQ method combines quantitative and qualitative evaluation to determine the surrounding rock grade. It is dominated by two independent quantitative indices, while other factors are incorporated through qualitative correction, making the method flexible and relatively easy to apply in engineering practice.

3. Tunnel Face Image-Recognition Method

3.1. Evaluation Index for Tunnel Face Integrity

The integrity of a tunnel face can be evaluated according to its fracture density. Rock mass fracture density commonly includes two forms. The first is the two-dimensional fracture density, also called the areal fracture density, which is the total length of fractures per unit area of the rock mass surface. The second is the three-dimensional fracture density, or volumetric fracture density, which is the sum of fracture areas per unit volume of rock mass. These two indices are calculated by Equations (3) and (4):

$$K_m = \sum_{i=1}^{n} l_i \Big/ A \tag{3}$$

$$K_V = \sum_{i=1}^{n} A_i \Big/ V \tag{4}$$

where l_i and A_i are the length and area of the i-th fracture in a unit area or unit volume, respectively; n is the number of fractures in the rock mass; A and V are the surface area and volume of the rock mass, respectively; and K_m and K_v are the areal and volumetric fracture densities, respectively.

Equations (3) and (4) show that fracture density is mainly related to the length and area of joints and fractures, but it cannot describe the connectivity among fractures. In practical engineering, the use of fracture density alone to evaluate tunnel face integrity has limitations. Therefore, by considering the combined influence of relevant factors, a crack ratio K_s is proposed as an index for evaluating tunnel face integrity, as shown in Equation (5). The integrity of the tunnel face is then evaluated according to the classification standard in Table 5.

$$K_s = k \sum_{i=1}^{n} A_i \Big/ A_z \tag{5}$$

where K_s is the crack ratio; k is a fitting parameter, obtained by least-squares experimental calibration using data source; A_i is the area of the i-th fracture in the tunnel face image (m^2); and A_z is the area of the tunnel face image (m^2).

Table 5. Classification of the crack ratio K_s.

Condition	Crack Ratio K_s				
	>0.1	**0.08–0.1**	**0.04–0.08**	**0.01–0.04**	**<0.01**
Joint and fracture development	Very	Developed	Moderately	Slightly	Undeveloped
Tunnel face integrity	Extremely fractured	Fractured	Relatively fractured	Relatively intact	Intact

3.2. YOLOv8-Based Localization and Detection of Joints and Fractures

3.2.1. YOLOv8 Algorithm

Deep learning models have strong feature-learning capability and end-to-end training characteristics, and they have shown great potential in object detection. The YOLO (You Only Look Once) model is characterized by fast detection and robust functionality and can satisfy the requirements of different application scenarios. The YOLO series transforms object detection into an end-to-end learning problem within a single neural network. Compared with traditional object-detection methods, it is simple, fast, and accurate. In this study, YOLOv8 was selected to localize joints and fractures on tunnel faces because of its favorable detection accuracy and computational efficiency.

3.2.2. YOLOv8 Dataset

The tunnel face images used in this study were collected from the Yueyang Laimipo Tunnel, the Lingdao Expressway tunnel. We have re-divided the dataset at the original-image level before augmentation. The original 600 images were split into [X] training images, [Y] validation images, and [Z] test images. Data augmentation was applied only to the training set. No augmented version of a training image appears in the validation or test set. We have retrained the model and updated all reported results accordingly. After redundant background information, such as machinery and workers, was cropped, 600 tunnel face images meeting the requirements were obtained. Because the image resolutions and sizes differed, the sample set was expanded and enhanced through geometric transformation, color transformation, noise addition, and size normalization to meet the requirements of deep learning training. A Python script (Python 3.10) was used to augment and enhance the existing samples, and 3600 tunnel face images were ultimately obtained. The images were randomly saved to the train, val, and test folders under the image directory, and the corresponding txt label files were saved to the train, val, and test folders under the label directory. The YOLOv8 dataset was thereby completed. Eighty percent of the images were used as the training set, 10% as the validation set, and the remaining 10% as the test set.

To accelerate convergence and improve generalization, pretrained weights and stochastic gradient descent (SGD) were adopted to mitigate overfitting. The training set was used to tune the model parameters and obtain the optimal weights, and the test set was then used to evaluate the trained model. The hyperparameters used during training are listed in Table 6.

Table 6. Experimental hyperparameter settings.

Parameter	Image Size	Epochs	Batch Size	Optimizer	Learning Rate	Momentum	Weight Decay
Value	640 × 640 × 3	300	4	SGD	0.01	0.937	0.0005

3.2.3. Detection-Result Analysis

The trained model was tested using the test set. Some target-detection results were used to evaluate the model. Figure 1 shows that the YOLOv8 algorithm can accurately identify the locations of joints and fractures and that no obvious missed detections occur. Overall, YOLOv8 is feasible for identifying and localizing joints and fractures on tunnel faces.

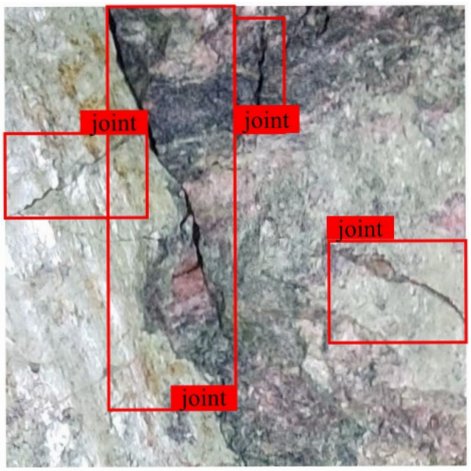


Figure 1. YOLOv8 detection results.

The algorithm was further evaluated using quantitative metrics. The precision-recall (PR) curve was first used to assess model performance. In general, a PR curve closer to the upper-right corner indicates better model performance and more reliable prediction results. As shown in Figure 2, the PR curve of the model is generally concentrated near the right side, indicating high recognition accuracy and good performance for fracture localization.

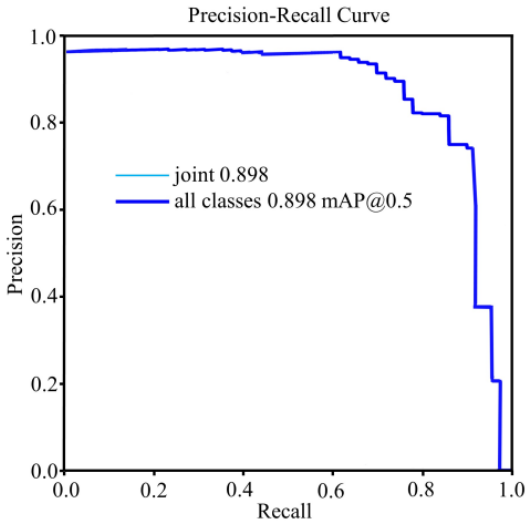


Figure 2. Precision-recall (PR) curve of YOLOv8.

The mean average precision (mAP) was also used as a comprehensive evaluation index. Because the model only detects the "fracture" class, mAP is equal to AP and represents the area enclosed by the PR curve. The mAP value was 0.898 (>0.8%, normally regarded as a good result), indicating that YOLOv8 achieved good recognition performance for joints and fractures on tunnel faces.

3.3. Quantitative Analysis of Joints and Fractures

3.3.1. Image Processing of Tunnel Face Fractures

According to Equation (5), calculation of the crack ratio requires the total fracture area in the tunnel face image. This area can be obtained through digital image processing. The workflow is shown in Figure 3.

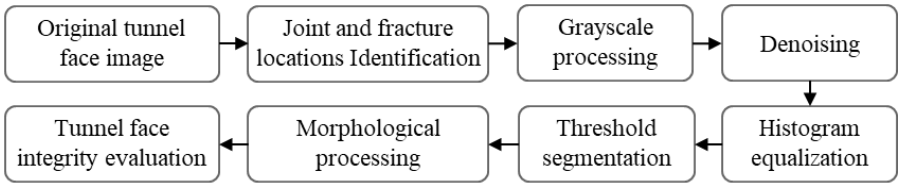
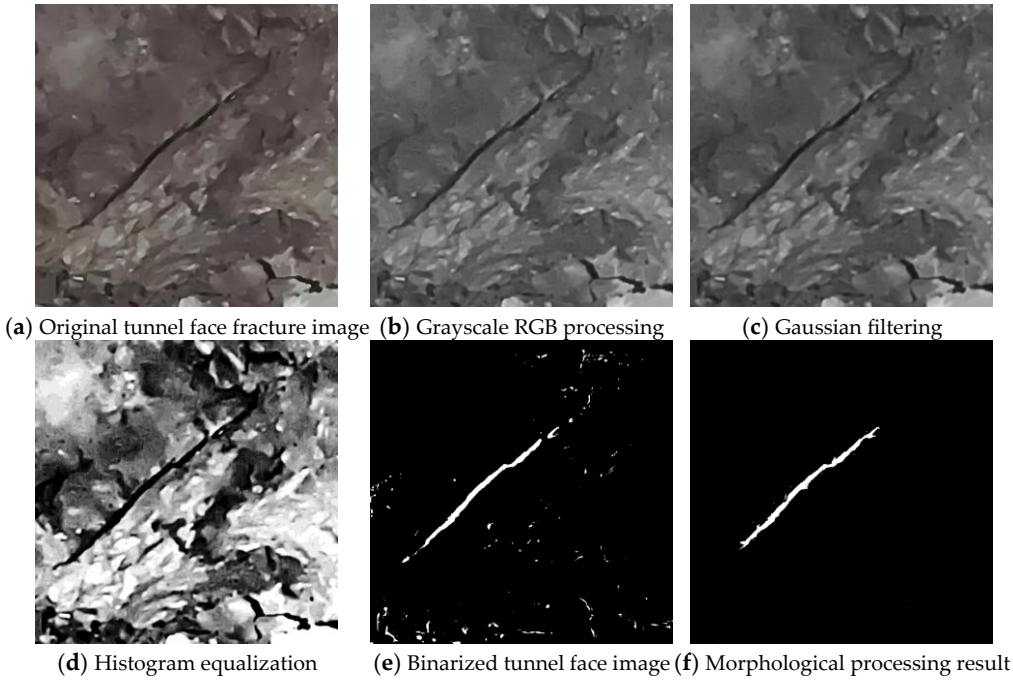


Figure 3. Workflow for evaluating tunnel face integrity.

Tunnel face photographs collected underground are often affected by uneven illumination, shadows, and brightness differences, which interfere with fracture-information extraction and increase post-processing complexity. Therefore, after joints and fractures are localized using YOLOv8, the tunnel face photographs containing fractures are subjected to grayscale conversion, denoising, histogram equalization, image binarization, and morphological processing. These steps remove irrelevant information, highlight the main image features, facilitate subsequent analysis, and reduce the computational burden.

Denoising is mainly performed by bilateral filtering, Gaussian filtering, and mean filtering to reduce or eliminate noise and improve image quality and clarity. Histogram

equalization expands the grayscale-pixel range from approximately 25–180 to 0–250, enhancing image contrast and facilitating subsequent extraction of joints and fractures. Image binarization is performed by combining the Canny algorithm with adaptive-threshold binarization for tunnel face image segmentation. Morphological processing is based on mathematical morphology and uses operations such as erosion, dilation, opening, and closing to change image shape, structure, and characteristics. The fracture-image processing procedure is shown in Figure 4.



(**a**) Original tunnel face fracture image (**b**) Grayscale RGB processing (**c**) Gaussian filtering

(**d**) Histogram equalization (**e**) Binarized tunnel face image (**f**) Morphological processing result

Figure 4. Processing procedure for tunnel face photographs.

3.3.2. Area Calculation of Joints and Fractures

After processing, only the regions occupied by joints and fractures are white, while the background region is black. Python code can therefore be used to identify the number of white or non-black pixels and calculate the fracture area. The image size is 640 × 640 pixels, and the total number of pixels is 409,600. For the same image, the area represented by each pixel is constant; therefore, the fracture-area ratio can be calculated by dividing the number of non-black pixels by 409,600.

The image-size information is included in the calculation procedure; thus, the ratio between the fracture area and the image area can be automatically obtained. We have added a complete parameter table for the image-processing procedure. This includes the filter type and kernel size, histogram equalization parameters, Canny thresholds, adaptive threshold window size and constant, morphological operation type, kernel size, and number of iterations. Algorithm 1 is used here. The corresponding pseudocode is presented Algorithm 1.

The calculation result can be substituted into Equation (5) to obtain the crack ratio K_s, and the tunnel face integrity can then be determined according to Table 5.

Algorithm 1. Fracture-area ratio calculation based on non-black pixel statistics

Input: Processed tunnel face fracture image I after binarization and morphological processing
Output: Number of non-black pixels N_f, total number of image pixels A_{img}, and fracture-area ratio R_f
Procedure:
1: Read the processed image $I \leftarrow$ cv2.imread(image_path)
2: Obtain image dimensions H, W, $C \leftarrow I$.shape
3: Initialize $N_f \leftarrow 0$
4: for $y = 1$ to H **do**
5: for $x = 1$ to W **do**
6: Extract pixel value p $\leftarrow I$(y, x)
7: if $p \neq (0, 0, 0)$ **then**
8: $N_f \leftarrow N_f + 1$
9: **end if**
10: **end for**
11: **end for**
12: Calculate $Aimg \leftarrow H \times W$
13: Calculate $R_f \leftarrow N_f / \mathrm{A_{img}}$
14: Return N_f, A_{img}, and R_f
Note: After morphological processing, non-black pixels are regarded as fracture pixels and black pixels are treated as the background.

4. Intelligent Classification Method for Tunnel Face Surrounding Rock

To rapidly obtain the surrounding rock grade during continuous tunnel construction, guide field construction in real time, reduce the occurrence of engineering accidents, and lower construction costs, this study proposes a rapid classification method based on the modified BQ approach. The two most important parameters in the BQ method are the saturated uniaxial compressive strength R_c and the rock mass integrity. These indices are usually obtained through testing, which is inconvenient for rapid field construction. A more convenient method is therefore needed for quantitative evaluation of rock hardness.

4.1. Acquisition of Tunnel Face Compressive Strength Rc

The final BQ value depends strongly on the estimated compressive strength. The saturated uniaxial compressive strength R_c of a rock mass is generally obtained directly through a uniaxial compression test or indirectly through a point-load test. However, because underground engineering construction is often continuous, it is difficult to obtain R_c rapidly and classify the surrounding rock in real time. To address this issue, the rebound strength of the tunnel face can be obtained on site and used to estimate R_c indirectly. The rebound value is related to rock hardness: harder rock generally produces a larger rebound value, while softer rock produces a smaller value. Thus, the rebound value can reflect rock quality to some extent. By analyzing the relationship between the rebound value and the saturated uniaxial compressive strength, R_c can be inferred indirectly, providing a convenient method for evaluating rock mechanical properties and supporting tunnel-construction safety.

During rebound testing on the tunnel face, the following principles should be followed. First, the selected test areas should be representative of the overall surrounding rock condition at the tunnel face. Second, multiple measurements should be conducted in each test area, and the test points should be distributed as uniformly as possible to reduce

experimental error. Third, the test areas and test points should avoid obvious cracks, cavities, and other damaged zones, and the tested surface should be flat and clean. As shown in Figure 5, three test areas are selected at the upper, lower-right, and lower-left parts of the tunnel face, forming a triangular layout. Each test area is approximately a 40 cm × 40 cm square and may be adjusted according to the size of the tunnel face. Sixteen test points are evenly distributed in each test area.

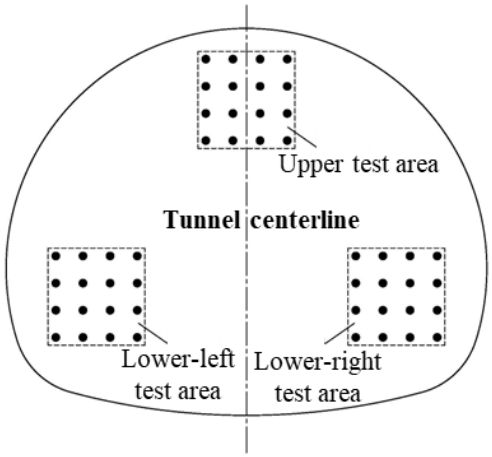


Figure 5. Layout of rebound test areas and points on the tunnel face.

According to the Technical Specification [25], the average rebound value of a test area is calculated as follows:

$$R_m = \frac{1}{10}\sum_{i}^{10} R_i \tag{6}$$

where R_m is the average rebound value of the test area, and R_i is the rebound value of the i-th test point.

After the average rebound value is obtained from Equation (6), it should be converted into saturated uniaxial compressive strength for the calculation of BQ. If the dry density of the rock is known, the empirical equation proposed by Müller in 1965 can be used, as shown in Equation (7):

$$\lg\sigma_c = 0.00863\rho_d N + 1.01 \tag{7}$$

where ρ_d is the dry density of the rock (g/cm^3); N is the rebound value; and σ_c is the compressive strength of the rock (MPa).

If the dry density of the rock is unknown, empirical Equations (8) and (9) may be adopted for claystone and non-claystone, respectively [26].

(1) Claystone:

$$R_c = 1.289e^{0.0631x} \tag{8}$$

(2) Non-claystone:

$$R_c = 20.013e^{0.0224x} \tag{9}$$

where R_c is the uniaxial saturated compressive strength (MPa), and x is the rebound value.

4.2. Acquisition of the Tunnel Surrounding Rock Grade

In practical engineering, it is usually difficult to rapidly obtain the rock mass integrity coefficient and the volumetric joint count. To achieve rapid classification during construction, the proposed method extracts information from tunnel face images, evaluates tunnel

face integrity, and maps the crack ratio K_s to the integrity coefficient K_v. Where K_v is obtained by the square of the elastic wave speed through the rock mass divided by the elastic wave speed through the rock block. The obtained K_v value is then substituted into the [BQ] calculation. In this way, rapid classification of tunnel surrounding rock can be achieved. The relationship between K_s and K_v is listed in Table 7, and the intelligent classification workflow based on tunnel face images is shown in Figure 6.

Table 7. Relationship between crack ratio K_s and integrity coefficient K_v (MHURDPRC, 2014) [7].

Integrity Degree of Tunnel Face	Extremely Fractured	Fractured	Relatively Fractured	Relatively Intact	Intact
Crack ratio K_s	>0.1	0.08–0.1	0.04–0.08	0.01–0.04	<0.01
Integrity coefficient K_v	<0.15	0.15–0.35	0.35–0.55	0.55–0.75	>0.75

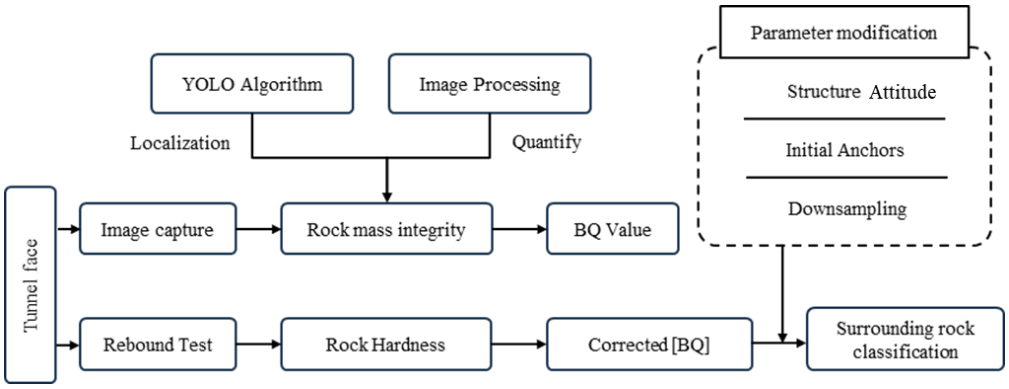


Figure 6. Workflow for intelligent surrounding rock classification.

5. Engineering Application

5.1. Project Overview

The proposed classification method was applied to the Laimipo Tunnel in Yueyang, Hunan Province. The tunnel is a shallow-buried, extra-large-span, double-hole multi-arch short tunnel with a total length of 275 m. The overall excavation span exceeds 36 m, including the central pilot tunnel; the width of a single bore is 15.75 m, and the clearance height is 5 m. The tunnel is shallowly buried; the surrounding rock has poor stability, and the maximum burial depth of the crown is less than 55 m, which is smaller than the critical depth between shallow and deep burial. The portal section is an ultra-shallow-buried construction section with a risk of collapse. To ensure construction safety, the tunnel was excavated using the central pilot tunnel first and then the double-side-drift method for the main tunnel.

The section from K1 + 735 to K1 + 810 was selected for study. This section mainly passes through strongly weathered carbonaceous siliceous slate of the Upper Sinian Doushantuo Formation (Z_{z2d}), underlain by moderately weathered carbonaceous siliceous slate of the same formation. The overlying strata include silty clay of the Quaternary Pleistocene residual-slope deposit (Qp^{el+dl}) and Holocene plain fill (Q_h). Joints and fractures are developed in the tunnel body, and the surrounding rock has poor conditions and low self-stability. The distribution of the rock and soil layers is shown in Table 8.

The tunnel site mainly contains pore water in Quaternary loose deposits and fissure water in bedrock. Pore water is mainly distributed in gravelly soil within the overburden, where permeability and water content are poor, and the water volume is small. Bedrock fissure water is mainly distributed in the carbonaceous siliceous slate strata and fault-fractured rock zones, both of which are weakly permeable layers. The groundwater amount

in this area is generally limited; the water table is deeply buried, and the stable groundwater level is 6.7–30.3 m below the ground surface. The main recharge source is atmospheric precipitation. In addition, ponds near the tunnel may cause potential seepage effects.

Table 8. Distribution of rock and soil layers.

No.	Rock/Soil Layer	Lithological Characteristics	Thickness (m)
1	Plain fill	Yellow, purplish-red and other colors; loose structure; mainly composed of cohesive soil mixed with slate fragments; self-weight consolidation not completed	3–4.5
2	Silty clay	Brownish-yellow to brownish-red; hard-plastic state; contains a small amount of gravel	0.5–3.5
3	Strongly weathered carbonaceous siliceous slate	Gray-brown to brownish-yellow; most minerals are weathered and altered; the rock is relatively soft, the rock mass is extremely fractured, and the core is mostly fragmented or blocky; local weathering is uneven, with a small amount of residual siliceous rock blocks	32–45
4	Moderately weathered carbonaceous siliceous slate	Dark-gray to gray-black; relatively hard to hard rock; fractured rock mass; the core occurs as fragments, blocks and a small number of short columns	Bedrock

Overall, the geological conditions of the Laimipo Tunnel are poor, the tunnel structure and stress state are complex, and the influences of groundwater and surface-water seepage may threaten construction stability. It is therefore necessary to dynamically classify the surrounding rock in this tunnel to provide a basis for timely adjustment of excavation and support measures.

5.2. Prediction and Validation of Intelligent Surrounding Rock Classification

The intelligent classification of the surrounding rock at the tunnel face was performed using the method described above. The procedure includes rebound testing on the tunnel face to indirectly obtain the rock-hardness index R_c, image recognition and processing to obtain the rock mass integrity coefficient K_v, and qualitative determination of the three correction coefficients, including the groundwater influence coefficient. The correction coefficients K_1–K_3 were independently determined according to the actual geological and hydrogeological conditions at the site, rather than being directly copied from the predicted column. Therefore, the comparison in Table 9 mainly evaluates the agreement between the estimated R_c and K_v and the code-based measured values, and further compares the final [BQ] classification results. It should be noted that if identical correction coefficients were used in both columns, the comparison cannot be regarded as an end-to-end independent validation of the BQ classification model, but mainly as a check of the estimation accuracy of R_c and K_v. This limitation has been stated in the manuscript. To verify the accuracy and reliability of the method, ten tunnel faces from the left and right bores of the Laimipo Tunnel were selected for classification prediction and compared with the actual classification. Table 9 compares the predicted and measured [BQ] values, and Figure 7 shows the detailed classification results.

Table 9. Comparison between predicted and measured [BQ] values. Source(s): Authors' own work.

No.	Tunnel Chainage	R_c (MPa)	K_v	K_1	K_2	K_3	Predicted [BQ]	Measured [BQ]	Quality Grade
1	K1 + 740	20.6	0.3	0.6	0.2	0	146.8	145	V
2	K1 + 756	60.6	0.7	0.3	0.2	0	406.8	418	III
3	K1 + 764	61.1	0.5	0.3	0.2	0.3	370.8	380	III
4	K1 + 770	47.3	0.5	0.6	0.2	0	276.9	270	IV
5	K1 + 778	60.7	0.48	0.6	0.2	0	312.1	315	IV
6	K1 + 785	40.5	0.5	0.2	0.2	0	306.5	305	IV
7	K1 + 791	60.4	0.75	0.3	0.2	0	418.7	418	III
8	K1 + 799	21.3	0.3	0.6	0.2	0	138.9	135	V
9	K1 + 803	60.2	0.66	0.3	0.2	0.3	345.6	380	III
10	K1 + 810	60.1	0.51	0.6	0.2	0	317.8	315	IV

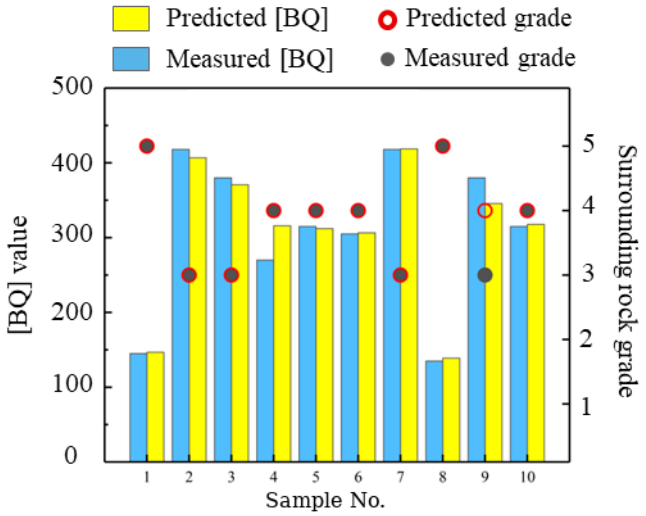


Figure 7. Comparison of predicted and measured [BQ] values and surrounding rock grades.

As shown in Figure 7 and Table 9, only one of the ten tunnel face samples was misclassified. In K1 + 803, the predicted BQ is 345.6, and the quality grade is IV, but the measured BQ is 380 and the quality grade is III; a grade III surrounding rock sample was predicted as grade IV. The corresponding [BQ] values were close to the classification boundary. All other samples were classified correctly, giving an accuracy of 90%. Overall, the proposed rapid surrounding rock classification method agrees well with the actual results. The method can satisfy the requirements for classifying surrounding rock near the tunnel face during continuous tunnel construction and can provide a reference for excavation and support.

6. Conclusions

Based on the YOLOv8 deep learning algorithm and digital image processing technology, this study takes the tunnel face as the research object and combines the modified BQ method to propose an intelligent rapid classification method for tunnel surrounding rock based on tunnel face images during construction. The method was applied to the Yueyang Laimipo Tunnel and showed good field performance. The main conclusions are as follows:

(1) The YOLOv8 deep learning algorithm can accurately identify and localize fractures on tunnel face photographs. The model exhibited good detection performance, and its mean average precision (mAP) value for the fracture class was 0.898. Combined with image processing and Python-based pixel calculation, the method can effectively

extract the fracture area, calculate the crack ratio Ks, and support quantitative analysis of tunnel face integrity.

(2) Based on the modified BQ method, a tunnel face integrity evaluation index based on the crack ratio K_s is proposed. By combining the deep learning algorithm and image processing, an intelligent method capable of rapid and accurate surrounding rock classification during continuous tunnel construction is established. The field application in the Laimipo Tunnel showed that the proposed method achieved a classification accuracy of 90%, satisfying the demand for rapid surrounding rock classification during construction and providing a reference for tunnel excavation and support.

Although the proposed method can rapidly classify the surrounding rock grade based on tunnel face photographs during construction, it depends on clear tunnel face imaging and rebound testing. In different tunnels, uncertainty may exist in the relationship between rebound values and measured compressive-strength values. Therefore, in subsequent applications, this relationship should preferably be calibrated through field or laboratory tests according to the actual conditions of each tunnel to improve classification accuracy.

Author Contributions: Conceptualization, J.F. and F.S.; methodology, F.S.; software, F.S.; validation, C.X.; formal analysis, J.F.; investigation, J.F.; resources, J.F.; data curation, C.X.; writing—original draft preparation, W.L.; writing—review and editing, J.F.; visualization, F.S.; supervision, W.L.; project administration, W.L.; funding acquisition, J.F. All authors have read and agreed to the published version of the manuscript.

Funding: This work was financially supported by the National Natural Science Foundation of China (52478424).

Institutional Review Board Statement: Not applicable.

Informed Consent Statement: Not applicable.

Data Availability Statement: The data presented in this study are available on request from the corresponding author.

Acknowledgments: The authors give thanks to the editors and anonymous reviewers for their constructive comments.

Conflicts of Interest: The authors declare no conflicts of interest.

References

1. Wang, H.; Guo, X.; Wu, Y.; Ma, H. Excavation Responses and Reliability of Soft Rock Tunnels Considering Spatial Variability Based on Copula Theory. *Eng. Comput.* **2026**, *43*, 2161–2181. [CrossRef]
2. Wei, G.; Mu, Z.; Feng, W.; Qi, Y.; Guo, B. Effects of Foundation Pit Excavation on Adjacent Metro Stations and Shield Tunnel Structures: A Study on Horizontal Displacement. *Eng. Comput.* **2024**, *41*, 2356–2380. [CrossRef]
3. Wickham, G.E.; Tiedemann, H.R.; Skinner, E.H. *Support Determinations Based on Geologic Predictions*; Society for Mining, Metallurgy & Exploration: Englewood, CO, USA, 1972; Volume 1.
4. Engineering Rock Mass Classifications: A Complete Manual for Engineers and Geologists in Mining, Civil, and Petroleum Engineering: Amazon.Co.Uk: Bieniawski, Z.T.: 9780471601722: Books. Available online: https://www.amazon.co.uk/Rock-Mass-Classifications-Geologists-Engineering/dp/0471601721 (accessed on 15 September 2026).
5. Barton, N.; Lien, R.; Lunde, J. Engineering Classification of Rock Masses for the Design of Tunnel Support. *Rock Mech.* **1974**, *6*, 189–236. [CrossRef]
6. Deere, D.U.; Hendron, A.J.; Patton, F.D.; Cording, E.J. Design of Surface and Near-Surface Construction in Rock. In *Proceedings of the 8th U.S. Symposium on Rock Mechanics (USRMS), Minneapolis, MN, USA, 15–17 September 1966*; OnePetro: Richardson, TX, USA, 1966.
7. *GB/T 50218-2014*; Standard for Engineering Classification of Rock Mass. China Planning Press: Beijing, China, 2014.
8. *GB 50287-2016*; Code for Hydropower Engineering Geological Investigation. China Planning Press: Beijing, China, 2016.

9. Tu, W.; Li, L.; Li, S.; Shi, S.; Zhou, Z.; Chen, D. Research on the Application of Dynamic Weighting on the Rock Mass Quality Rating. *Arab. J. Geosci.* **2019**, *12*, 87. [CrossRef]
10. Jiang, F.; Gao, C.; He, P.; Wang, G.; Zheng, C.; Xiao, Z.; Wu, Y.; Yuan, W. Research on a Method for Evaluating Rock Mass Quality Based on Fuzzy Reasoning and Support Vector Machines. *Appl. Geophys.* **2026**, *23*, 1–16. [CrossRef]
11. He, P.; Chen, Y.; Jiang, F.; Wang, G.; Jiang, Y. An Approach to Rapidly Evaluating Rock Mass Quality in Underground Engineering Based on Multi-Source Heterogeneous Data. *Rock Mech. Rock Eng.* **2025**, *58*, 1295–1325. [CrossRef]
12. Aydan, Ö.; Ulusay, R.; Tokashiki, N. A New Rock Mass Quality Rating System: Rock Mass Quality Rating (RMQR) and Its Application to the Estimation of Geomechanical Characteristics of Rock Masses. *Rock Mech. Rock Eng.* **2014**, *47*, 1255–1276. [CrossRef]
13. Sun, F.; Huang, G.-B.; Jonathan Wu, Q.M.; Song, S.; Wunsch, D.C., II. Efficient and Rapid Machine Learning Algorithms for Big Data and Dynamic Varying Systems. *IEEE Trans. Syst. Man Cybern. Syst.* **2017**, *47*, 2625–2626. [CrossRef]
14. Wen, X.; Fan, Y.; Sun, F.; Zhang, X.; Sun, K.; Xiao, H.; Liu, P. A Novel Model of Fuzzy Rough Set with Applications in Data Classification and Image Segmentation. *Appl. Soft Comput.* **2026**, *191*, 114677. [CrossRef]
15. Sun, S.; Li, S.; Li, L.; Shi, S.; Liu, H.; Hu, J.; Zhou, S. Structural Planes Surveying and Fractal Dimension Characteristics of Tunnel Face Based on Digital Photogrammetry. *Arab. J. Geosci.* **2018**, *11*, 622. [CrossRef]
16. Hou, D.; Zheng, X.; Zhou, Y.; Gong, C.; Wang, C. Analysis and Application of Surrounding Rock Mechanical Parameters of Jointed Rock Tunnel Based on Digital Photography. *Geotech. Geol. Eng.* **2023**, *41*, 721–739. [CrossRef]
17. Ma, J.; Ma, C.; Li, T.; Yan, W.; Faradonbeh, R.S.; Long, H.; Dai, K. Real-Time Classification Model for Tunnel Surrounding Rocks Based on High-Resolution Neural Network and Structure–Optimizer Hyperparameter Optimization. *Comput. Geotech.* **2024**, *168*, 106155. [CrossRef]
18. Zhang, S.; Chen, Z.; Ling, T.; Huang, N.; Zhang, L. A Dynamic Classification Method for Surrounding Rock Based on the Fusion of Tunnel Face Images and Ground Penetrating Radar Advanced Geological Forecast Images. *Meas. Sci. Technol.* **2025**, *36*, 106104. [CrossRef]
19. Chen, J.; Zhang, D.; Huang, H.; Shadabfar, M.; Zhou, M.; Yang, T. Image-Based Segmentation and Quantification of Weak Interlayers in Rock Tunnel Face via Deep Learning. *Autom. Constr.* **2020**, *120*, 103371. [CrossRef]
20. Zhang, W.; Zhang, W.; Zhang, G.; Huang, J.; Li, M.; Wang, X.; Ye, F.; Guan, X. Hard-Rock Tunnel Lithology Identification Using Multi-Scale Dilated Convolutional Attention Network Based on Tunnel Face Images. *Front. Struct. Civ. Eng.* **2023**, *17*, 1796–1812. [CrossRef]
21. Liu, Q.; Yan, J.; Li, H.; Zhang, P.; Liu, Y.; Liu, L.; Ye, S.; Liu, H. Intelligent Identification of Surrounding Rock Grades Based on a Self-Developed Rock Drilling Test System. *Buildings* **2024**, *14*, 2176. [CrossRef]
22. Niu, W.; Chen, J.; He, B.; Xiong, Y.; Jin, Z. Intelligent Identification Method for Hard Structural Planes in Surrounding Rocks of Deep Tunnels. *J. Rock Mech. Geotech. Eng.* **2026**, *18*, 2725–2742. [CrossRef]
23. Xu, C.; Wang, C.; Li, M.; Liu, X. An Intelligent Recognition and Classification Method for TBM Tunnel Surrounding Rock Based on Cross-Attention Transformer and Multi-Source Data Fusion. *Int. J. Rock Mech. Min. Sci.* **2026**, *200*, 106438. [CrossRef]
24. *JTG 3370.1-2018*; Specification for Design of Highway Tunnels (I) Civil Engineering. China Communications Press: Beijing, China, 2018.
25. *JGJ/T 23-2011*; Technical Specification for Inspecting Concrete Compressive Strength by Rebound Method. China Architecture & Building Press: Beijing, China, 2011.
26. Deng, X.F.H. *Research on Rapid Classification of Tunnel Surrounding Rock and Intelligent Control of Over-Under-Excavation Blasting (Chinese Edition)*; Science Press: Beijing, China, 2022.

Disclaimer/Publisher's Note: The statements, opinions and data contained in all publications are solely those of the individual author(s) and contributor(s) and not of MDPI and/or the editor(s). MDPI and/or the editor(s) disclaim responsibility for any injury to people or property resulting from any ideas, methods, instructions or products referred to in the content.